THE JOURNAL OF BIOLOGICAL CHEMISTRY VOL. 286, NO. 18, pp. 16470–16481, May 6, 2011

The Crystal Structure of the *Leishmania major* Deoxyuridine Triphosphate Nucleotidohydrolase in Complex with Nucleotide Analogues, dUMP, and Deoxyuridine*[S]

Received for publication, January 25, 2011, and in revised form, February 25, 2011 Published, JBC Papers in Press, March 15, 2011, DOI 10.1074/jbc.M111.224873

Glyn R. Hemsworth[‡], Olga V. Moroz[‡], Mark J. Fogg[‡], Benjamin Scott[‡], Cristina Bosch-Navarrete[§], Dolores González-Pacanowska[§], and Keith S. Wilson[‡1]

From the [‡]Structural Biology Laboratory, Department of Chemistry, University of York, Heslington, York YO10 5DD, United Kingdom and the [§]Instituto de Parasitología y Biomedicina "López-Neyra," Consejo Superior de Investigaciones Científicas, Granada, 18100 Armilla, Spain

Members of the *Leishmania* genus are the causative agents of the life-threatening disease leishmaniasis. New drugs are being sought due to increasing resistance and adverse side effects with current treatments. The knowledge that dUTPase is an essential enzyme and that the all α-helical dimeric kinetoplastid dUTPases have completely different structures compared with the trimeric β-sheet type dUTPase possessed by most organisms, including humans, make the dimeric enzymes attractive drug targets. Here, we present crystal structures of the *Leishmania major* dUTPase in complex with substrate analogues, the product dUMP and a substrate fragment, and of the homologous *Campylobacter jejuni* dUTPase in complex with a triphosphate substrate analogue. The metal-binding properties of both enzymes are shown to be dependent upon the ligand identity, a previously unseen characteristic of this family. Furthermore, structures of the *Leishmania* enzyme in the presence of dUMP and deoxyuridine coupled with tryptophan fluorescence quenching indicate that occupation of the phosphate binding region is essential for induction of the closed conformation and hence for substrate binding. These findings will aid in the development of dUTPase inhibitors as potential new lead anti-trypanosomal compounds.

Various members of the genus *Leishmania* cause leishmaniasis, which threatens ~350 million people worldwide and gives rise to about two million clinical cases each year, of which ~25% are of the fatal visceral form (1). The disease is largely endemic to developing countries, and current treatments are expensive and can result in undesirable side effects for the patient (1). This, combined with the increasing drug resistance that is developing in the *Leishmania* species, means that new and novel anti-parasitic drug targets are urgently required.

Deoxyuridine triphosphate nucleotidohydrolase (dUTPase)[2] represents such a target. dUTPases catalyze the hydrolysis of dUTP to dUMP and pyrophosphate (2). This provides the starting material for the synthesis of dTMP by thymidylate synthase and in addition maintains the ratio of dTTP:dUTP in the cell at a high enough level to prevent excessive misincorporation of dUMP into the genome during DNA replication (3). dUTPase activity is essential as was shown by gene knock-outs in *Escherichia coli* and *Saccharomyces cerevisiae*. Inhibition of dUTPase activity results in futile cycles of DNA repair that ultimately cause the fragmentation of DNA and cell death (4, 5). dUTPase activity also appears to be essential in *L. major* (6) and the related parasite *Trypanosoma brucei*, where an RNAi approach was used to knock down dUTPase expression, resulting in decreased cell proliferation and growth in both procyclic and bloodstream forms of the organism (7).

dUTPases have been characterized extensively both biochemically and structurally in many species. Most organisms, including humans, have trimeric dUTPases with structures largely consisting of β-pleated sheet (8). Three active sites are formed at the trimer interfaces by five characteristic sequence motifs. Each subunit contributes to every active site present in the trimer, with a single divalent metal ion bound in each of the active sites in the presence of substrate (9, 10). This metal ion has been implicated in substrate binding and catalysis as the presence of Mg^{2+} reduces the K_m of the *E. coli* enzyme by a 0.5 to 1 order of magnitude and increases the value of k_{cat} 2- to 3-fold in the *Drosophila melanogaster* enzyme (11, 12). Monomeric dUTPases also have been identified that appear to have arisen by gene duplication merging two protomers of the trimeric enzyme into a single polypeptide (13). These monomeric enzymes are found only in mammalian herpes viruses and have the same five characteristic sequence motifs as the trimeric enzymes but in a different order.

The enzymes from *L. major* (*Lm*dUTPase), *Trypanosoma cruzi* (*Tc*dUTPase), and *Trypanosoma brucei* (*Tb*dUTPase) as

* This work was funded by European Union Grant agreement 223238, Spanish Plan Nacional Grant SAF2007-62596, FIS Network Grant RD06/0021, and the Junta de Andalucía Grant CVI-199.

[S] The on-line version of this article (available at http://www.jbc.org) contains supplemental Figs. 1–3.

The atomic coordinates and structure factors (codes 2CJE, 2CIC, 2YAY, 2YAZ, and 2YB0) have been deposited in the Protein Data Bank, Research Collaboratory for Structural Bioinformatics, Rutgers University, New Brunswick, NJ (http://www.rcsb.org/).

[1] To whom correspondence should be addressed: Structural Biology Laboratory, Department of Chemistry, University of York, Heslington, York YO10 5DD, UK. E-mail: keith@ysbl.york.ac.uk.

[2] The abbreviations used are: dUTPase, deoxyuridine triphosphate nucleotidohydrolase; *Lm*dUTPase, dUTPase from *L. major*; *Tc*dUTPase, dUTPase from *T. cruzi*; *Tb*dUTPase, dUTPase from *T. brucei*; *Cj*dUTPase, dUTPase from *C. jejuni*; dUTP, 2′-deoxyuridine 5′-triphosphate; dUDP, 2′-deoxyuridine 5′-diphosphate; dUMP, 2′-deoxyuridine 5′-monophosphate; dU, 2′-deoxyuridine; dUpNpp, α,β-imino-deoxyuridine triphosphate; dUpNp, α,β-imino-deoxyuridine diphosphate; r.m.s.d., root mean square deviation(s); TLS, Translation Libration Screw-motion.

well as some bacterial species show markedly different structural and biochemical properties to the trimeric enzymes (14). These enzymes act as dimers and are able to hydrolyze not only dUTP but also dUDP (15), whereas dUDP has been shown to be an inhibitor of the trimeric enzyme in *E. coli* (16). They are, in addition, subject to product inhibition by dUMP (17). The structure of *Tc*dUTPase revealed a dimeric all α-helical structure that is very distinct from the trimeric enzymes (18), with which they share no sequence similarity. The dimeric dUTPases also have five sequence motifs responsible for forming the active site, but these are quite different from those in the trimeric dUTPases. The structure of the *T. cruzi* enzyme has been determined in the apo open form and in the closed form in complex with dUDP (18). These structures revealed a large conformational change in the protein upon substrate binding with the mobile domain moving as much as 20 Å with the concomitant rearrangement of secondary structure elements in this domain. Subsequently, a structure of the closed form of the dimeric dUTPase from *Campylobacter jejuni* (*Cj*dUTPase) was determined in the presence of the nonhydrolyzable substrate analogue dUpNp (19). This revealed the presence of three Mg^{2+} ions in the active site adjacent to the phosphate groups of the substrate. The metals were implicated in substrate binding and led to the proposal that these dimeric dUTPases utilize a mechanism of reaction similar to that used in the phosphoryl transfer reactions catalyzed by DNA polymerases (20, 21). Indeed, the dimeric enzyme, like the trimeric one, requires divalent metal ions for activity (17).

The essential nature of dUTPases and the marked differences between the two forms of the enzyme in different species make the dimeric dUTPases an attractive target for anti-parasitic drug development. With this in mind, we have undertaken a structural characterization of the *L. major* dUTPase in complex with various substrate fragments to better understand the substrate binding determinants and the requirements to induce closure of this family of enzymes. Here, we present crystal structures of the closed *L. major* dUTPase in the presence of the non-hydrolyzable substrate analogues α,β-imino-deoxyuridine triphosphate (dUpNpp) and α,β-imino-deoxyuridine diphosphate (dUpNp) and divalent metal ions supporting the proposed mechanism for these dimeric enzymes. Subsequent structures with deoxyuridine monophosphate (dUMP) and deoxyuridine (dU) bound reveal a completely closed conformation with sulfate ions bound to the enzyme, showing the importance of the negatively charged 5′ region of the substrate to induce enzyme closure. We also present the structure of the *Cj*dUTPase in complex with dUpNpp with important implications for the metal-binding properties of this family of enzymes.

EXPERIMENTAL PROCEDURES

Cloning and Expression of L. major dUTPase—The coding sequence for the dimeric dUTPase from *L. major* 252 was amplified by PCR, using genomic DNA as template, and cloned. For expression, two constructs were created using the forward primers *Lm*DUT3C-F (5′-CCAGGGACCAGCAATGAAGCGCGCTCGCAGC-3′) and *Lm*DUTLIC-F (5′-CACCACCACCACATGAAGCGCGCTCGCAGC-3′) with the reverse primer *Lm*DUT-R (5′-GAGGAGAAGGCGCGTTATGCCTTGATCGCCAGCCG-3′) common to both constructs. The underlined overhangs were included to allow cloning into the pET-YSBL3C and pET-YSBLLIC vectors, respectively (22). 0.2 pmol of PCR product were treated with T4 DNA polymerase (New England Biolabs) in the presence of dATP to produce large overhangs for cloning into the Ligation Independent Cloning vectors. The Ligation Independent Cloning vector was linearized with the restriction enzyme BseRI and treated with T4 DNA polymerase in the presence of 2′-deoxythymidine 5′-triphosphate to produce complementary overhangs to the PCR product. The PCR product and the vector were then mixed in a 2:1 ratio of insert to vector and allowed to anneal at room temperature for 30 min. The mixture was then used to transform NovaBlue singles competent cells (Novagen). Colonies were picked and grown in 5-ml cultures overnight. Plasmids were isolated from cells using the Qiagen mini-prep kit, and the presence of insert in the vector confirmed by sequencing from the T7 promoter. The vectors were designated pET-*Lm*DUT3C and pET-*Lm*DUTLIC. BL-21 (DE3) competent cells were then transformed with these vectors to allow protein expression. Six 500-ml cultures derived from a single colony of BL-21 (pET-*Lm*DUT3C) or BL-21 (pET-*Lm*DUTLIC) were grown in LB medium containing 30 μg/ml kanamycin at 37 °C to an A_{600} of 0.6–0.8. Expression of dUTPase was then induced by the addition of isopropyl 1-thio-β-D-galactopyranoside to a final concentration of 1 mM, and the temperature was lowered to 25 °C for the *Lm*DUT3C construct but maintained at 37 °C for the *Lm*DUTLIC construct, as these were the conditions determined to be optimal for soluble expression of protein in small scale expression trials. After 4 h, cells were harvested by centrifugation at 8000 rpm in a Sorvall F-10 rotor for 20 min. The cell paste was stored at −20 °C until required for purification.

Purification of L. major dUTPase—Typically ~2.5 g of cell paste were resuspended in 10× volumes of lysis buffer (50 mM HEPES, pH 7.0, 50 mM NaCl, 5 mM $MgCl_2$, 1 mM PMSF), and cells were lysed using three 10-s pulses of sonication at maximum amplitude using an MSE Soniprep 150 sonicator. Cell debris was removed by centrifugation at 18,000 rpm in a Sorvall SS-34 rotor for 20 min at 4 °C. Supernatants were removed and applied to a 5-ml GE Healthcare HiTrap nickel-nitrilotriacetic acid column that had been equilibrated in Buffer A (50 mM HEPES, pH 7.0, 50 mM NaCl, 5 mM $MgCl_2$, 1 mM imidazole). The column was washed with 3 column volumes of Buffer A before a 50-ml gradient of Buffer B (Buffer A + 300 mM imidazole) was applied to elute the protein. 5-ml fractions were collected along the gradient. For the *Lm*DUT3C construct, peak fractions containing the enzyme were pooled for treatment with human rhinovirus 3C protease (Novagen). 1 unit of protease was added per mg of dUTPase, and the solutions were incubated at 4 °C overnight. The protein was concentrated using a 10-kDa molecular mass cut off Millipore concentrator by centrifugation at 4 × *g* to a volume of ~1 ml. The protein was diluted 10-fold with Buffer A to dilute the imidazole, and the protein was applied back onto the nickel column used in the previous step. The flow-through was collected, and the column was washed with 2 column volumes of Buffer A. The untagged protein was in the flow-through, which was concentrated to ~1 ml for gel filtration. The *Lm*DUTLIC construct lacks the 3C

protease site and therefore was concentrated following the initial nickel column for gel filtration. Gel filtration was performed in the same way for both constructs using a GE Healthcare 16/60 HiLoad Superdex S75 column, which had been equilibrated with gel filtration buffer (10 mM HEPES, pH 7.0, 200 mM NaCl, 5 mM $MgCl_2$). Following a void volume of 45 ml, 2.5-ml fractions were collected. Fractions containing *Lm*dUTPase were combined, and the buffer was exchanged into 10 mM HEPES, pH 7.0, 5 mM $MgCl_2$ on a Millipore concentrator. The *Lm*DUT-3C and *Lm*DUTLIC protein samples were concentrated to 80 mg/ml and 15 mg/ml, respectively, as judged by the absorbance at 280 nm using an extinction coefficient of 53,900 M^{-1} cm^{-1} for both proteins. 50-μl aliquots of protein were flash-frozen under liquid nitrogen and stored at −80 °C for future use.

Crystallization of L. major dUTPase in Complex with dUpNp and dUpNpp—The *Lm*DUTLIC sample was used for crystallization with the dUpNp substrate analogue (Jena Biosciences). Prior to crystallization, dUpNp was added to the protein to a final concentration of 2 mM. Initial crystallization trials were performed using a Mosquito robot (TTP Labtech) leading to crystals in the Index screen (Hampton Research), condition G10: 0.2 M $MgCl_2$, 0.1 M Bis-Tris, pH 5.5, 25% PEG-3350. However, these were small clusters of needles that were unsuitable for x-ray analysis and step-by-step seeding was used to increase the size. The clusters were crushed using a needle and were used to seed fresh hanging drops set up in similar conditions with a precipitant range of 20–25%. Bigger crystals grew following this procedure, which was repeated until diffraction quality crystals were obtained. Finally, single crystals were obtained in 20% PEG MME 3350, 0.2 M $MgCl_2$, 0.1 M Bis-Tris, pH 5.5.

For the dUpNpp complex, *Lm*DUT3C protein at 70 mg/ml was mixed with an equal volume of 10 mM dUpNpp to give final concentrations of 35 mg/ml protein and 5 mM ligand. Initial crystallization trials were set up as for the dUpNp complex leading to crystals in the PACT screen (Molecular Dimensions), condition B11: 0.2 M $CaCl_2$, 0.1 M MES, pH 6.0, 20% PEG-6000. Repeating the condition in larger hanging drops varying the concentration of PEG-6000 from 15–25% yielded quality crystals suitable for data collection.

Crystallization of L. major dUTPase in Complex with dUMP and dU—The *Lm*DUT3C protein was used for crystallization of both the dUMP and dU complexes. To form the 2′-dUMP complex, 2.5 μl of a 200 mM nucleotide stock was diluted 20-fold with 80 mg/ml protein to yield a final concentration of 10 mM dUMP and 76 mg/ml protein. To obtain the dU complex, protein was mixed with a 200 mM stock of 2′-dU and a 0.5 M stock of sodium pyrophosphate (PP_i) to give final concentrations of 10 mM dU, 10 mM PP_i, and 75 mg/ml dUTPase. Initial crystallization trials were set up using a Mosquito robot as for the other complexes. Crystals of both complexes grew in the same condition in the index screen (Hampton Research), condition C6: 0.1 M NaCl, 0.1 M Bis-Tris, pH 6.5, 1.5 M $(NH_4)_2SO_4$. Larger crystals were then obtained in hanging drop vapor diffusion experiments using the same condition but varying the $(NH_4)_2SO_4$ concentration over the range of 1.0–2.0 M.

X-ray Data Collection, Processing, and Structure Determination for L. major dUpNp and dUpNpp Complexes—Crystals of the dUpNp complex were cryo-cooled to 120 K using 30% PEG-3350, 0.2 M $MgCl_2$, 0.1 M Bis-Tris, pH 5.5, as the cryo-protectant. Data were collected at the European Synchrotron Radiation Facility (Grenoble, France; station ID29) (wavelength 0.97 Å) and processed using DENZO and SCALEPACK to 2.34 Å resolution in the space group $P6_522$ with cell dimensions $a = b = 87.9$ Å, $c = 146.5$ Å, and $\gamma = 120.0°$. The dUDP-bound structure of the *T. cruzi* enzyme was used as the search model for molecular replacement using MOLREP (23). Following an initial refinement with REFMAC (24), a partial model was constructed using ARP/wARP (25). This was completed manually over several rounds of rebuilding and refinement using COOT (26) and REFMAC, respectively. The TLS option was utilized in REFMAC, splitting the rigid and mobile domains of the protein into three TLS groups. In the later stages of refinement, the contribution of hydrogen atoms to the structure factors was taken into account. The results of refinement are shown in Table 1.

dUpNpp complex crystals were cryo-cooled to 120 K using mother liquor supplemented with 15% ethylene glycol as the cryo-protectant. Data were collected from these crystals at the European Synchrotron Radiation Facility (station ID14-2) at a fixed wavelength of 0.933 Å. Images were indexed using iMosflm (27), which showed they belonged to the same space group as the dUpNp complex crystals. Data were scaled and merged using SCALA (28) to a resolution of 1.9 Å. The Free-R set was taken from the dUpNp complex data and extended to higher resolution for use in structure refinement. The starting model was the dUpNp structure after removing ligand, solvent molecules, and flexible loops formed by residues 61–68, 195–205, and 212–217. The structure was rebuilt and refined using COOT and REFMAC5. TLS refinement was performed again, using the same TLS groups as used earlier and also including hydrogens later in the refinement.

X-ray Data Collection, Processing and Structure Determination for dUMP and dU Complexes—Data were collected from crystals of the dUMP and dU complexes at station IO4 of the Diamond Light Source at a wavelength of 0.976 Å. Images were indexed using iMosflm and integrated in the space group *P*3. POINTLESS (28) identified the point group as $P3_121$ or $P3_221$. Data were reindexed into both these space groups and were scaled using SCALA to 2.4 Å resolution for the dUMP complex and 2.3 Å for the dU complex crystals (see Table 1 for scaling and refinement statistics). The structure of the dUMP complex was determined by molecular replacement with MOLREP using the dUpNp complex determined previously as the search model with the ligand, solvent molecules, and the flexible loops formed by residues 61–68, 195–205, and 212–217 were removed to avoid bias. Searches were performed in both $P3_121$ and $P3_221$ with a good solution identified in $P3_121$ with four protomers in the asymmetric unit. The crystals grown in the presence of dU and PP_i were isomorphous to the dUMP crystals, and so this molecular replacement solution was also used as a starting point for the dU structure. The models were refined and rebuilt using REFMAC5 and COOT. Two TLS groups were defined for each protomer in the asymmetric unit using the TLSMD server

(29). The quality of the model was checked throughout model building and refinement using MolProbity (30). The Protein Data Bank codes are shown in Table 1.

Crystallization of C. jejuni dUTPase in Complex with dUpNpp—Protein was purified as described in Moroz *et al.* (19). Briefly, recombinant protein was purified in a two-step procedure consisting of a phosphocellulose column followed by size exclusion chromatography. Purified protein was concentrated to 15 mg/ml, and buffer was exchanged into 10 mM HEPES, pH 7.0. Protein was mixed with dUpNpp to yield a final concentration of 2 mM prior to setting up crystallization screens in the same way as for the *L. major* dUTPase. Initial microcrystals were obtained in the index screen, condition C1: 3.5 M sodium formate, pH 7.0. These crystals were optimized manually with the addition of 20 mM magnesium acetate to produce diffraction quality crystals.

X-ray Data Collection, Processing, and Structure Determination for C. jejuni dUpNpp Complex—Crystals were cryo-cooled to 120 K in a nitrogen stream from an Oxford Cryosystems device using 3.5 M sodium formate, pH 7.0, 12.5% glycerol as a cryo-protectant. Crystals belonged to the space group $I4_122$, with cell dimensions $a = b = 93.4$ Å and $c = 143.6$ Å, and data were collected to 1.7 Å resolution at the European Synchrotron Radiation Facility beamline BM14. There was a single subunit in the asymmetric unit with a V_M of 2.9 Å^3/Da and a solvent content of 57%. Data were processed using DENZO and SCALEPACK (31) before structure determination by molecular replacement in MOLREP using the *C. jejuni* dUpNp complex structure as the search model. The model was completed manually using the XFIT option of the program QUANTA (Accelrys, San Diego, CA) and refined using REFMAC with the TLS option. The rigid and mobile domains of *Cj*dUTPase were used as two separate TLS groups. Processing and refinement statistics are shown in Table 1.

Tryptophan Fluorescence Quenching—Titrations monitoring the tryptophan fluorescence of *L. major* dUTPase were performed using a Horiba Jobin Yvon Fluoromax-4 spectrofluorometer with a 5-mm path length quartz cuvette. The dUTPase was present in solution at a dimer concentration of 1 μM to which 1 μl of concentrated ligand was added per injection. The solutions were mixed thoroughly and allowed to equilibrate for 1 min before measurements were taken. An excitation wavelength of 295 nm was used, and fluorescence was measured at 330 nm using excitation and emission slit widths of 2 and 3 nm, respectively. The buffer used throughout the experiments was 10 mM HEPES, pH 7.0, with either 5 mM $MgCl_2$ or 1 mM EDTA. When pyrophosphate was used in the measurements, it was present at a concentration of 1 mM. Data for the dU and dUMP titrations were plotted and analyzed using SigmaPlot in a similar manner to that used by Ortiz-Salmeron *et al.* (32). No significant inner filter effects were experienced due to the ligands used during the course of this work.

For the dUpNpp titrations where the ligand to protein concentration ratio was lower, data were fitted to the quadratic equation below,

$$F_{\text{norm}} = B_m - B_q\{(L_0 + M_0 + K_d) - \sqrt{(L_0 + M_0 + K_d)^2 - 4L_0M_0}\} \quad \text{(Eq. 1)}$$

where F_{norm} is the normalized protein fluorescence, B_m is the maximum protein fluorescence, B_q is the fluorescence change upon ligand binding, L_0 is the ligand concentration corrected for dilution, M_0 is the protein concentration corrected for dilution, and K_d is the dissociation constant for the ligand.

RESULTS

L. major dUTPase Overall Fold—The structure was determined in two different crystal forms. The dUpNp and dUpNpp complexes were in space group $P6_522$ with a single protomer in the asymmetric unit (Table 1). Structures of the dUMP and dU complexes were in space group $P3_121$, with two dimers in the asymmetric unit (Table 1). The structures in both space groups are very similar with the protomer in $P6_522$ superimposing with each protomer in $P3_121$ with r.m.s.d. of 0.67, 0.60, 0.78, and 0.65 Å over 257 residues for chains A, B, D, and E, respectively.

The *Lm*dUTPase protomer is made up of 10 α-helices (residues 11–29, 32–35, 38–53, 70–92, 135–150, 154–168, 172–188, 218–222, 224–242, and 252–262) linked by flexible loops (Fig. 1*A*). Two domains were identified previously in the *Tc*dUTPase structure, a "rigid" domain that mediates the dimerization and a "mobile" domain that undergoes significant domain movement upon substrate binding (18). Similar to *Cj*dUTPase, *Lm*dUTPase structures could only be determined in the closed form, but the domains can be defined similarly (Fig. 1*A*). The rigid domain is formed by residues 32–169 and the mobile domain by residues 8–31 and 170–265. In the *Tc*dUTPase structure, there were two regions that could not be modeled in the mobile domain, residues 94–103 and 119–139 (18). There was good density for the equivalent loops (residues 94–103 and 117–125, respectively) in *L. major*, so most of the sequence could be modeled into the electron density with the exception of the first eight N-terminal residues in most of the structures and two residues at the very C terminus that are likely to be flexible.

*Lm*dUTPase, similar to the *T. cruzi* (18) and *C. jejuni* (19) enzymes, is a dimer (Fig. 1*B*), with dimerization largely mediated via the rigid domains of the protein. In the $P6_522$ crystals, the dimer is formed about a crystallographic 2-fold symmetry axis burying 5530 Å^2 and 5700 Å^2 of surface area in the dUpNpp and dUpNp complexes, respectively. In $P3_121$, there are two dimers in the asymmetric unit with 5380 Å^2 (chains A and B) and 5530 Å^2 (chains C and D) surface area buried in the dUMP complex and 5790 Å^2 (chains A and B) and 5500 Å^2 (chains C and D) surface area buried in the dU complex. In all of the structures, a loop from one subunit reaches over to contact the ligand in the other member of the dimer. The interactions at the dimer interface in the *Cj*dUTPase were slightly different to those of the *T. cruzi* enzyme (18). The interactions at the interface in *L. major* resemble those of the *T. cruzi* enzyme with many of the residues here conserved between the two species (Fig. 1*C*).

CjdUTPase dUpNpp Complex Structure—We sought to obtain further information on binding of the triphosphate moiety by determining the *Cj*dUTPase dUpNpp complex, following our earlier study of the closed structure of the dUpNp complex (19). The

TABLE 1

Data Processing and Refinement Statistics for the *Lm* and *Cj*dUTPase Structures

Statistics in parentheses represent data in the highest resolution shell. The ΔB values refer to the difference in B values between pair of bonded atoms.

Data Processing	*L. major*				*C. jejuni*
Dataset	**dUpNp**	**dUpNpp**	**dUMP**	**dU**	**dUpNpp**
Space Group	$P6_522$	$P6_522$	$P3_121$	$P3_121$	$I4_122$
Cell Dimensions					
a (Å) α (°)	87.9 90.0	86.8 90.0	109.1 90.0	109.2 90.0	93.4 90.0
b (Å) β (°)	87.9 90.0	86.8 90.0	109.1 90.0	109.2 90.0	93.4 90.0
c (Å) γ (°)	146.5 120.0	145.3 120.0	309.3 120.0	308.9 120.0	143.6 90.0
No. of molecules in asymmetric unit	1	1	4	4	1
Resolution (Å)	76.03-2.34 (2.40-2.34)	43.40-1.90 (2.00-1.90)	54.60-2.40 (2.53-2.40)	60.80-2.28 (2.40-2.28)	30.00-1.70 (1.75-1.70)
Beamline	ESRF ID29	ESRF ID14.2	Diamond I04	Diamond I04	ESRF BM14
Wavelength (Å)	0.976	0.933	0.976	0.976	0.980
Observed/unique refls	203,763/14,713	443,077/25,978	1,199,352/84,915	1,330,676/98,557	268,057/33,092
R_{merge} (%)	5.0 (29.8)	5.2 (91.3)	11.7 (91.6)	11.1 (70.6)	5.0 (29.8)
Multiplicity	13.8 (8.0)	17.1 (11.9)	14.1 (10.9)	13.5 (10.5)	8.1 (4.4)
Completeness (%)	99.9 (99.9)	99.0 (99.0)	100.0 (100.0)	100.0 (99.8)	97.8 (90.8)
Mean(I/σ(I))	28.0 (3.3)	30.1 (2.6)	16.5 (2.7)	17.4 (3.0)	37.1 (3.3)
Refinement Statistics					
Number of reflections (working/free sets)	13,849/737	25,688/1,353	80,604/4,239	93,350/4,921	31,466/1,700
Number of atoms	2,124	2,028	8,119	8,210	2,378
R_{work}/R_{free}	0.187/0.238	0.214/0.249	0.203/0.225	0.210/0.235	0.162/0.206
RMS deviation from ideality:					
Bond lengths (Å)	0.015	0.013	0.011	0.012	0.019
Bond angles (°)	1.50	1.47	1.31	1.38	1.93
Chiral Volume ($Å^3$)	0.096	0.091	0.093	0.087	0.199
Average B factors for all atoms ($Å^2$)	56.3	48.8	60.8	85.9	28.6
ΔB factors of bonded atoms ($Å^2$)					
Overall	1.61	9.0	3.8	4.2	1.4
Main chain	1.40	8.8	2.7	3.4	0.8
Side chain	1.86	9.2	5.2	5.2	2.0
Ramachandran plot. Proportion of residues in (%):					
favored regions	100.0	100.0	100.0	99.9	100.0
allowed regions	98.8	99.6	98.6	98.1	100.0
disallowed regions	0.0	0.0	0.0	0.1	0.0
PDB code	2cje	2yay	2yaz	2yb0	2cic

structure in complex with the triphosphate substrate analogue determined here belonged to a different crystal form (Table 1) with a single subunit in the asymmetric unit, the dimer being formed about a crystallographic 2-fold symmetry axis. The protomer in the *Cj*dUTPase dUpNpp complex can be superimposed onto that of the diphosphate analogue complex with an r.m.s.d. of 0.67Å over 223 α-carbons showing that the overall fold of the protein is essentially identical in the two complexes. The biggest difference between the two complexes is the presence of only two Mg^{2+} ions in the dUpNpp active site compared with three in the dUpNp complex. This will be discussed in more detail below.

Protein Ligand Interactions—Structures of *Lm*dUTPase were determined with four ligands bound (dUpNpp, dUpNp, dUMP, and dU). The interactions formed between the five sequence motifs of this family of enzymes and their substrates have been described previously (18, 19), and so will not be discussed in detail here. The five motifs form the active site in the same way as in the closed *Tc*dUTPase structure (Fig. 2*A*). The *Lm*dUTPase and *Cj*dUTPase dUpNpp complexes are the first structures for this family of enzymes to contain the triphosphate moiety. Both reveal that there are surprisingly few direct hydrogen bonds between the γ-phosphate of the substrate and the protein. Indeed, the only residue within hydrogen bonding distance of the γ-phosphate in *Lm*dUTPase is Glu^{51}, which is also involved in coordinating the catalytically important metal ions. The γ-phosphate makes two contacts in *Cj*dUTPase hydrogen bonding to Asn^{202} and Lys^{194}. These differences do not appear to be due to movements in side chain positions as these are well conserved between the two species but rather due to a different positioning of the γ-phosphate of the substrate (Fig. 2*B*). Therefore, it would appear that there is a degree of flexibility in the positioning of the γ-phosphate in the active site. This is additionally supported by the fact that the *B*-factors for the γ-phosphate atoms are higher than for the rest of the ligand, indicating a substantial degree of mobility.

The only other difference in ligand binding between *Cj*dUTPase and *Lm*dUTPase is at the bottom of the active site pocket adjacent to the O4 group of the uracil ring. In the *Cj*dUTPase complex, the O4 group hydrogen-bonds to the Nδ2 group of Asn^{21}. The equivalent residue in *L. major* is Asp^{29}, which has its side chain pointing away from the active site. This side chain is involved in a hydrogen-bonding network through water molecules to the O4 group of the uracil ring, resulting in the presence of a small water filled cavity at the bottom of the pocket, which is also seen in the *Tc*dUTPase. This feature might be exploitable in the development of new inhibitors of the kinetoplastid enzymes.

Sulfate Ions in Active Site—The aim of obtaining the dU- and dUMP-bound *Lm*dUTPase crystal structures was to determine whether the phosphate groups were required for closure of the enzyme upon binding. These complexes reveal that the interactions between the protein and the uracil and deoxyribose moieties are identical when these ligands are bound compared with dUpNpp and dUpNp. However, large tetrahedral electron density peaks were observed, which were interpreted as SO_4^{2-} ions from the crystallization medium (Fig. 2, *C* and *D*).

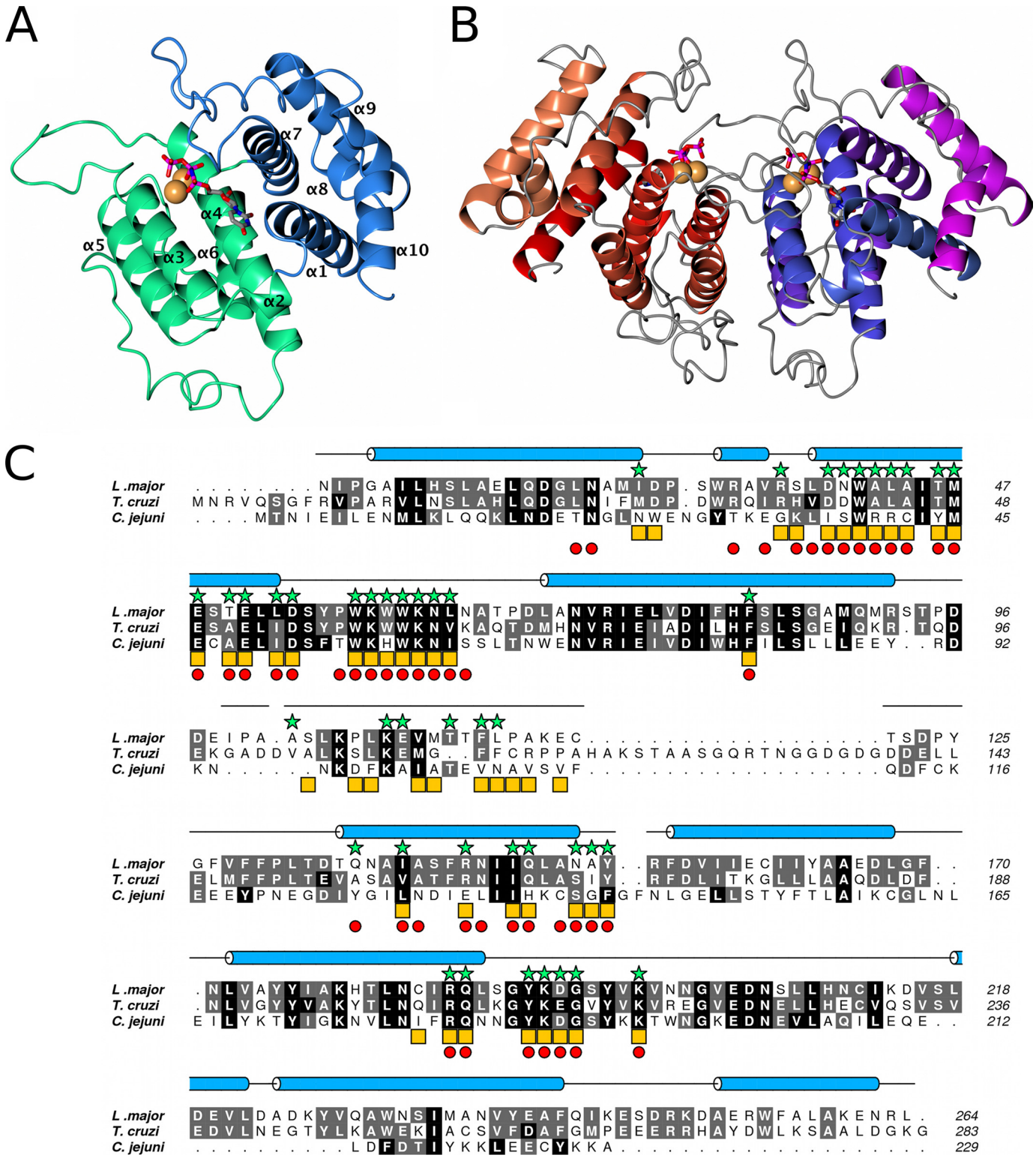

FIGURE 1. *A*, structure of the *Lm*dUTPase protomer. Secondary structures are numbered in order from the N to C terminus. The rigid domain is colored *green*, and the mobile domain is colored *blue*. *Orange spheres* represent the Ca^{2+} ions present in the active site adjacent to the dUpNpp ligand. (*Sticks* are colored by atom type.) *B*, the *Lm*dUTPase dUpNpp complex dimer formed about a crystallographic 2-fold. *C*, structure-based sequence alignment of *Lm*-, *Tc*- and *Cj*dUTPases. Residues that interact across the dimer inteface are highlighted with *green stars*, *orange squares*, and *red circles* in *Lm*-, *Tc*-, and *Cj*dUTPase, respectively, illustrating that the dimer interface in *Lm*dUTPase resembles more closely the interface in *T. cruzi* than in *C. jejuni*. All molecular graphics figures were generated using CCP4mg (35), and sequence alignments were made using ALINE (36).

In both of the dUMP and dU complexes, there was electron density for a tetrahedral group adjacent to the 5′ end of the ligand. These were modeled as sulfate ions (Fig. 2, *C* and *D*), based on the presence of ammonium sulfate as the crystallization precipitant. In the dUMP complex, a single sulfate was modeled into each of the four protomers. These sulfate ions

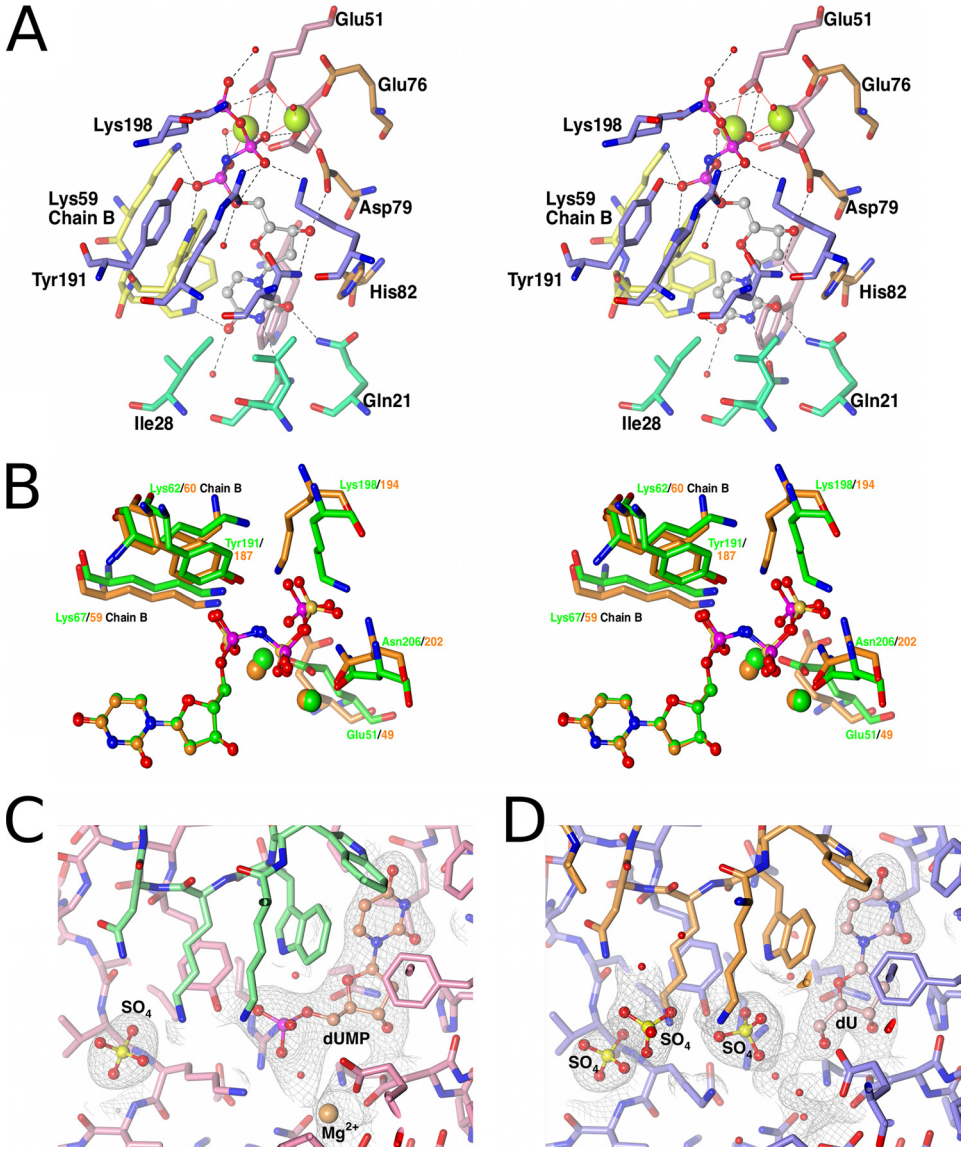

FIGURE 2. *A*, stereo diagram of the interactions between the *L. major* dUTPase and the substrate analogue dUpNpp (*ball and stick*). Protein residues are shown in *stick* representation colored by atom type with the carbon atoms from motif I colored *green*, motif II colored *pink*, motif III colored *yellow*, motif IV colored *orange*, and motif V colored *purple*. Calcium ions are shown as *green spheres*, and water molecules are shown as *smaller red spheres*. *Black dashed lines* show hydrogen bonds, and *red solid lines* show the metal coordination geometry. *B*, stereo diagram of the *Lm*- (*green* carbons, *magenta* phosphorous atoms) and CjdUTPase dUpNpp (*orange* carbon and phosphorous atoms) complexes superposed on their ligands giving an r.m.s.d. of 0.39 Å over 28 atoms. The γ-phosphates in the two complexes occupy slightly different positions, but the arrangement of the residues in contact with these groups shown as *sticks* are largely conserved between the two structures. *C* and *D*, regions of the $2F_{obs} - F_{calc}$ electron density maps for chain A of the *L. major* dUTPase in the presence of dUMP (*A*) and dU (*B*) contoured at 1σ (maps clipped at a 2.5 Å radius around the ligand, sulfates, and metal ion). Chain A is colored *pink* and *purple*, and chain B is colored *green* and *orange* in the dUMP and dU complexes, respectively.

hydrogen-bond to the side chains of Lys^{59}, Lys^{62}, and Asn^{63}, except in chain A, where the sulfate is positioned slightly differently and hydrogen-bonds to the side chain of Lys^{62}, and the main chain amide groups of Lys^{198} and Val^{199}; all of which are conserved among the kinetoplastid dimeric dUTPases (supplemental Fig. 1). Superposition of the various chains reveals that the loop formed by residues 198–205 occupies a different position in chain A, leading to this difference in positioning of the sulfate ion in this chain, a result of crystal packing as this loop mediates interactions with chain D of a symmetry related molecule (supplemental Fig. 2).

In the dU co-crystallizations, PP_i was added, as this was expected to aid binding of the dU moiety. Additional electron density present in the active site could not be modeled as PP_i and was again interpreted as sulfate ions (Fig. 2*D*). There were more sulfates than in the dUMP complex. Chains *B*, *D*, and *E* have two sulfates bound. One occupies a position intermediate to that taken up by the α- and β-phosphate groups of the longer substrate. This hydrogen bonds to a water molecule bridging it to the 5′-OH group of the dU moiety and the sidechains of Lys^{59}, Trp^{61}, Lys^{62}, Tyr^{191}, and Lys^{198}. The second sulfate binds in a similar position to that taken up by those in the equivalent chains of the dUMP complex. As in the dUMP complex, chain A differs from the other three protomers as it has three sulfate ions bound. Two of these are equivalent to those in the other chains, with the third occupying a similar position to that taken

up by the sulfate in chain A of the dUMP complex, which hydrogen-bonds to the main chain amide groups of Lys^{198} and Val^{199} and the side chain of Lys^{62}.

Identification of Metal Binding Sites—Use of non-hydrolyzable substrate analogues resulted in the binding of metal ions in the active sites. As the equivalent *Cj*dUTPase complex (19), the *Lm*dUTPase dUpNp contains three metal ions adjacent to the phosphate tail of the substrate. These were assigned as Mg^{2+}, based on the octahedral coordination geometry and bond lengths (33), and are coordinated by the side chains of four conserved acidic residues, Glu^{48} and Glu^{51} from motif II and Glu^{76} and Asp^{79} from motif IV. The phosphate groups of the dUpNp and water molecules provide the remaining metal coordination.

Both the *Lm*- and *Cj*dUTPases dUpNpp triphosphate analogue complexes surprisingly contained only two metal ions. The two metals in *Cj*dUTPase were again identified as Mg^{2+} on the basis of octahedral coordination geometry and bond lengths. There was an electron density peak ~1 Å from the third metal binding site in the dUpNp complex in both species, but it did not have coordination geometry consistent with a metal ion and was thus interpreted as a water molecule (Fig. 3, *A* and *B*). In the *Lm*dUTPase structure, the metal ions showed octahedral coordination geometry, but the bond lengths were slightly longer and were assigned as Ca^{2+} from the crystallization solution. Calculation of anomalous difference Fourier maps revealed two strong electron density peaks at these positions, confirming them as Ca^{2+} with no peak present that could represent a third calcium (supplemental Fig. 3). It would therefore appear that the presence of the γ-phosphate displaces the third metal ion from the active site.

A single Mg^{2+} ion was modeled into the active sites of three of the four protomers in the asymmetric unit in the dUMP complex. The electron density for these was somewhat weak, and the bond lengths were longer than would be expected for an Mg^{2+} ion. However, superposition of the dUMP bound structure with the dUpNp-bound structure shows that the Mg^{2+} modeled into the dUMP complex occupies a similar position to the central magnesium in the dUpNp complex coordinated by Glu^{48}, Glu^{76}, and Asp^{79}. In the dU complex, there was an electron density feature lying between the two metal ions in the dUpNpp complex. The bond lengths to this feature were too long, and the coordination geometry was not correct for it to be a magnesium. It was therefore modeled as a water, which hydrogen bonds to a sulphate ion.

Tryptophan Fluorescence Quenching—The presence of one of the sulfate ions in the dU complex at the phosphate binding region of the active site suggested that occupation of this site was likely to be an important factor in inducing closure of the enzyme around the substrate. To probe this further, binding assays were performed with dUpNpp, dUMP, and dU in the presence and absence of pyrophosphate, using tryptophan fluorescence quenching.

Representative binding curves are shown in Fig. 4. As would be expected, the affinity of the protein ligand interactions follows the pattern dUpNpp > dUMP > dU in the absence of pyrophosphate and in the presence of Mg^{2+}. Binding of all of the ligands is weakened severely in the absence of Mg^{2+}, indicating that it must play a role in dU binding, even though it was not seen in the crystal structure. The presence of pyrophosphate had a significant influence on the affinity of the enzyme for dU, reducing the dissociation constant from an immeasurably high value to 140 μM. In contrast, pyrophosphate had very little influence upon dUMP binding, with closely similar K_d values of 7.3 μM without PP_i and 17 μM in its presence. This suggests that the α-phosphate plays a major role in inducing closure of the enzyme, and from the point of view of inhibitor design, the presence of a negatively charged moiety, which would interact with the phosphate binding region of the protein, will be required to lock the protein into the higher affinity closed conformation.

DISCUSSION

Active Site and a Likely Mechanism of Action—The active sites of all of the dimeric dUTPase structures determined to date are very similar. The *T. cruzi* dUDP complex lacked metals in the active site, and so a mechanism of reaction could not be proposed (18). The subsequent structure of the *C. jejuni* enzyme bound to the diphosphate substrate analogue dUpNp revealed the presence of three Mg^{2+} ions adjacent to the phosphate groups of the substrate (19). Metals are clearly important for substrate binding (17), supported by the tryptophan fluorescence quenching experiments on the *L. major* enzyme (Fig. 4) and data reported previously (34). In the *C. jejuni* dUpNp complex (19), one of the water molecules coordinating the central Mg^{2+} ion was positioned in line with the scissile bond, leading to the suggestion that this was a likely nucleophile with the reaction proceeding by a similar two ion mechanism to that proposed for the phosphoryl transfer reactions performed by DNA polymerases and many other enzymes (20, 21).

We describe here the structure of *L. major* dUTPase in complex with the two substrate analogues dUpNpp and dUpNp (Fig. 3*A*). The positions of essentially all of the ligand atoms are close to identical in both complexes. There is a small rotation in the position of the β-phosphate. More importantly, there are only two metal ions (Ca^{2+}) in the dUpNpp structure. In the dUpNpp complex, the γ-phosphate causes a 0.8 Å movement of Glu^{51}, distorting the active site slightly, which is perhaps related to the loss of the third metal ion. The two structures are both in keeping with the previously proposed mechanism, with the catalytic water molecule positioned in the same place in both structures, but 0.2/0.4 Å from that in the *C. jejuni* dUpNp complex (Fig. 3*C*) (19).

It is curious that in the presence of the triphosphate substrate analogue, only two metal ions are bound in the active site. The *C. jejuni* dUpNpp complex reported here also only has two metal ions, although these are both Mg^{2+} ions. There is a more dramatic difference between the *C. jejuni* dUpNpp and dUpNp complexes, where the side chain of Glu^{49} (equivalent to Glu^{51} in *Lm*dUTPase) is flipped away from the active site in the presence of the triphosphate, such that it no longer coordinates any metal ions (Fig. 3*B*). This is quite different to its position in the *C. jejuni* dUpNp complex, and indeed, the two *Leishmania* complexes, where a much smaller movement of Glu^{51} was observed between the equivalent structures. The 0.8 Å shift in the position of Glu^{51} in the *Lm*dUTPase complex could result

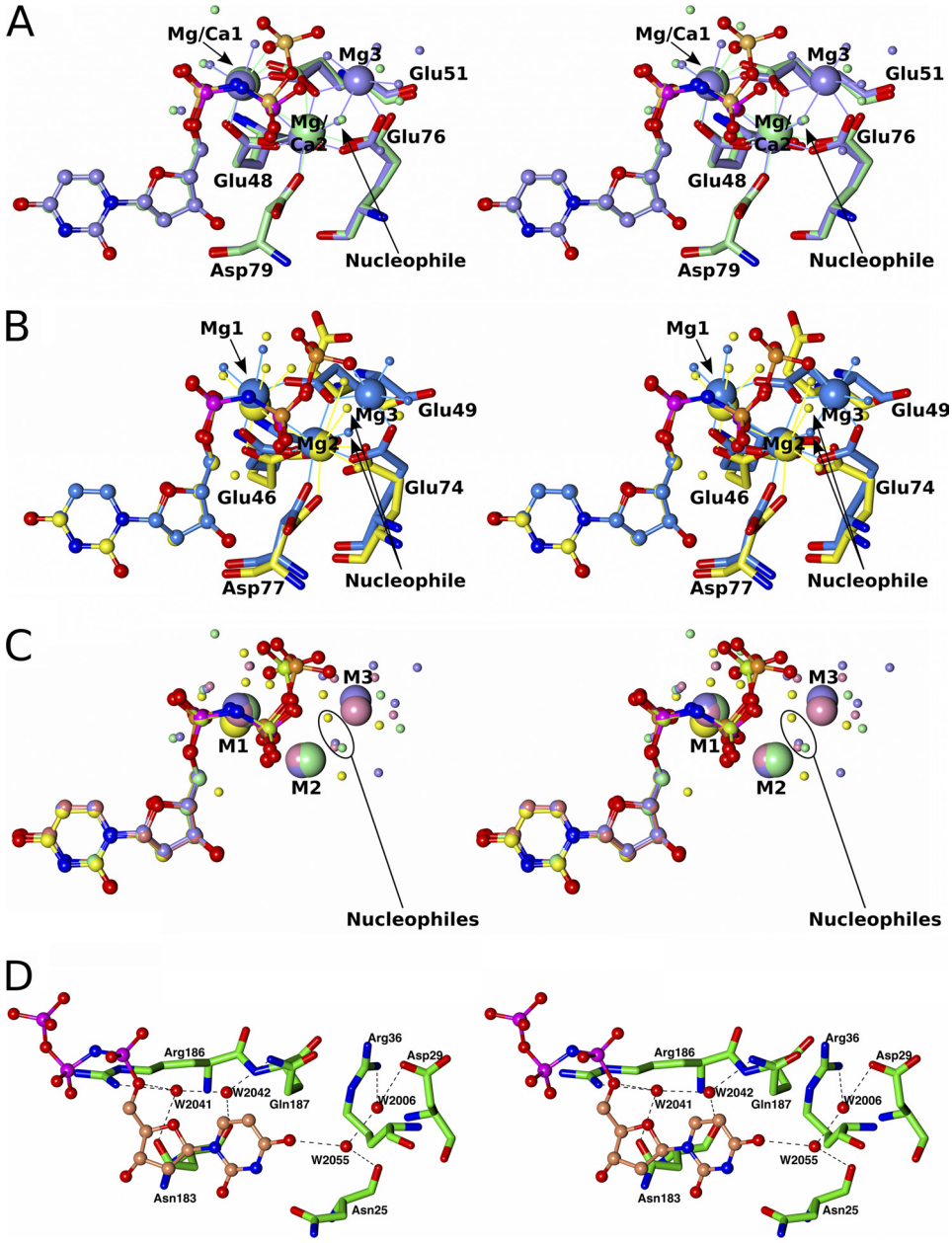

FIGURE 3. *A*, stereo view of the *L. major* dUpNpp (*green* carbons, *orange* phosphorous) and dUpNp (*purple* carbons, *magenta* phosphorous) complexes superposed. Ligands are shown as *ball and stick*, metals are shown as *large spheres*, and the protein residues coordinating the metals are shown as *sticks*. The water structures for the two complexes are shown with *smaller spheres* with their coordination geometry illustrated by *solid lines*. Structures were superposed using secondary structure matching giving an r.m.s.d. of 0.38 Å over 257 α-carbon positions. *B*, stereo view of the *C. jejuni* dUpNpp (*yellow* carbons, *orange* phosphorous) and dUpNp (*blue* carbons, *magenta* phosphorous) complexes superposed. Ligands, metals, water molecules, and protein residues are depicted in the same way as for *A*. Structures were superposed using the ligands with an r.m.s.d. of 0.18 Å over 24 atoms. *C*, stereo view of the superposition of *Cj*-dUpNp (*pink* carbons, *brown* phosphorous), *Cj*-dUpNpp (*yellow* carbons, *orange* phosphorous), and *Lm*-dUpNp (*purple* carbons, *magenta* phosphorous) complexes onto the *Lm*dUpNpp complex (*green* carbons and phosphorous). Superpositions were performed using the ligands giving r.m.s.d. values of 0.17 Å over 24 atoms, 0.39 Å over 28 atoms, and 0.18 Å over 24 atoms, respectively. *D*, stereo view of the *Lm*dUTPase active site showing the water molecules present in cavities adjacent to the substrate. Residues that contact these waters are shown as *sticks* colored by atom type, and the hydrogen bonds that the water molecules make are shown as *black dashed lines*.

from the presence of Ca^{2+} rather than Mg^{2+} in this structure, with the longer coordinating bond lengths causing the loss of the third metal site. However, the loss of the third metal site in the presence of the triphosphate substrate analogue is common to both enzymes, and so this appears to be a general feature of this family of enzymes. In addition, the presumed nucleophilic water is displaced by 1.2/1.5 Å from that observed in the two *Leishmania* structures.

The differing metal-binding properties depending upon the identity of the substrate may be necessary for the correct positioning of the nucleophile for attack on the scissile bond. In the presence of the diphosphate substrate, three metals are bound with the proposed catalytic water molecule coordinated by metals 2 and 3, aligning it for an in-line attack on the α–β-phosphate bond. In the presence of the triphosphate, the third metal is lost, but the proposed nucleophile is

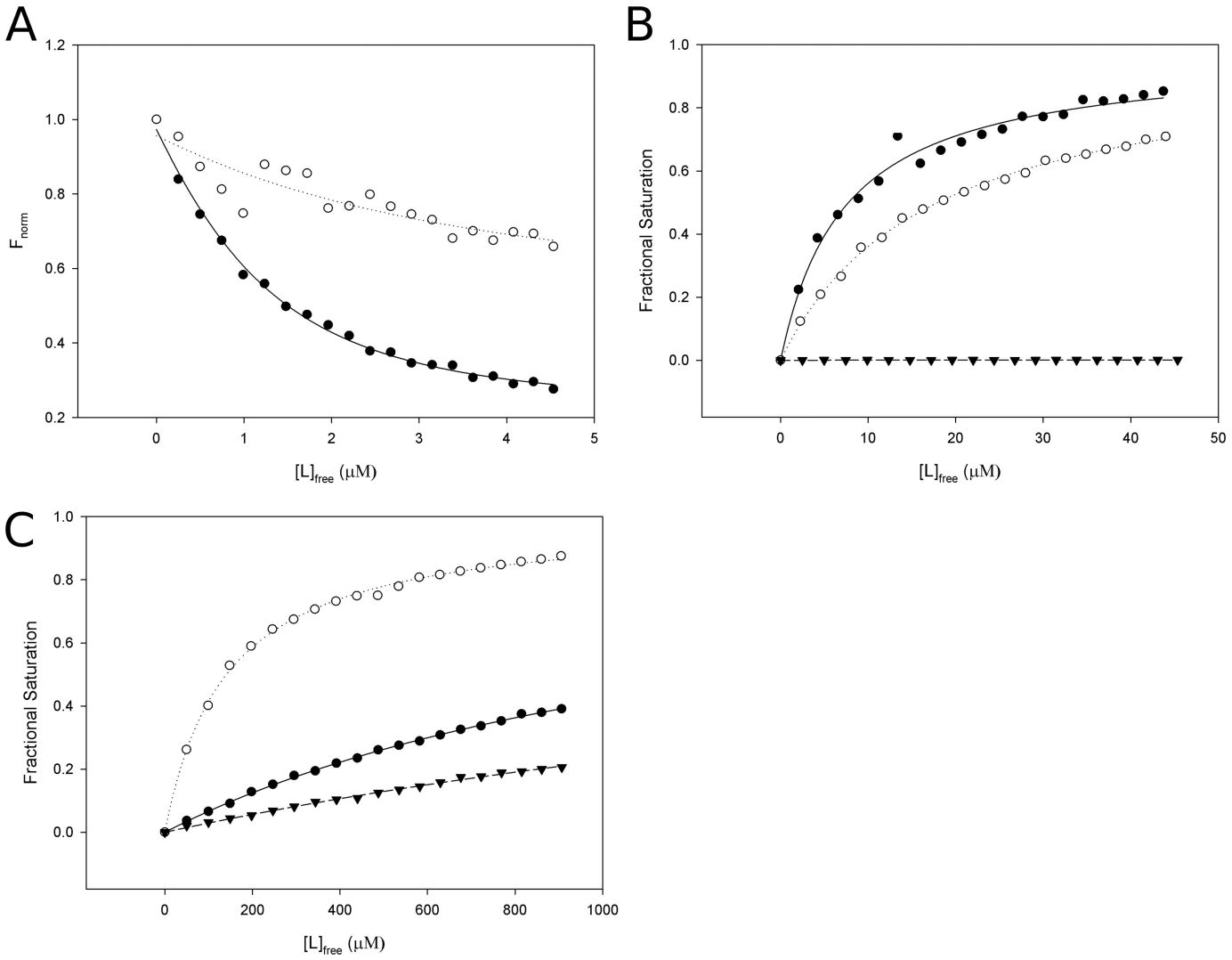

FIGURE 4. **Curves obtained for binding of ligands to the *Lm*dUTPase determined from tryptophan fluorescence quenching.** *A*, dUpNpp binding in the presence of Mg^{2+} (*filled circles*, K_d = 0.8 μM) and in its absence (*open circles*). *B*, dUMP binding in the presence of Mg^{2+} (*filled circles*, K_d = 7.3 μM), Mg^{2+} + PP_i (*open circles*, K_d = 17 μM), and in the absence of Mg^{2+} (*filled triangles*). *C*, dU binding in the presence of Mg^{2+} (*filled circles*), Mg^{2+} + PP_i (*open circles*, K_d = 140 μM), and in the absence of Mg^{2+} (*filled triangles*).

still present, albeit in a slightly different position to that in the diphosphate complex, ~0.3 Å away in the *Leishmania* and ~1.3 Å in the *C. jejuni* enzyme. The third metal ion may no longer be required, as the γ-phosphate itself aids in aligning the nucleophile for an in-line attack on the scissile bond. This certainly seems to hold for the *C. jejuni* enzyme; however, in the *Lm*dUTPase dUpNpp complex, the third phosphate group occupies a slightly different position to that taken up in the *C. jejuni* enzyme and is too far away from the proposed catalytic water to interact with it.

From an inhibitor design point of view, there is little space in or around the active site in the closed form of the enzyme to allow binding of substrate derivatives (Fig. 3*D*). One avenue that may be exploited is at the bottom of the ligand binding pocket. In the *C. jejuni* enzyme, there is an Asn residue that hydrogen-bonds to the O4 group of the uracil ring. In the kinetoplastids, this residue is replaced by an Asp, which is rotated away from the active site with the hydrogen bond to the O4 group of the substrate provided by a water molecule in both the *L. major* structures presented here and the *T. cruzi* dUDP complex. Thus, this deeper cavity could be exploited by a modification to the O4 group of the uracil ring. Another site for modification could be the water-occupied pocket adjacent to the deoxyribose moiety of the substrate (Fig. 3*D*). However, both of these positions pose certain difficulties in terms of synthetic chemistry. In principle, there is the possibility of modifying the phosphate moiety, but this was rather tightly packed against the surrounding protein.

Importance of Phosphate Groups for Enzyme Closure—Dimeric dUTPases represent a potential drug target and a better understanding of the requirements for enzyme closure will clearly aid in the design of new inhibitors. The structures of the *Lm*dUTPase in complex with the substrate fragment dU revealed a completely closed enzyme with sulfate ions from the crystallization liquor present in and near the active site. A single sulfate was observed in the dUMP complex, binding at a distinct site from that taken up by the other phosphate

groups of the larger substrate analogues. These sulfate ions are positioned 5–6.5 Å away from the phosphate group of the dUMP molecule and are bound by residues that are conserved among the dimeric dUTPases of the kinetoplastids (supplemental Fig. 1). This positioning may represent the site occupied by the pyrophosphate moiety following the reaction.

Sulfates occupy the same sites in the dU as in the dUMP complex with the exception of an additional sulfate, which binds in a position intermediate to that taken up by the α- and β-phosphate groups of the larger dUpNp and dUpNpp ligands (Fig. 2*D*). The presence of the sulfate ion here suggested that occupation of the phosphate binding region by a negatively charged group is likely to be important to induce closure of the enzyme. Tryptophan fluorescence quenching with the *Lm*dUTPase revealed that the presence of pyrophosphate had a marked influence on the dissociation constant for dU reducing the K_d from an immeasurable number to 140 μM (Fig. 4*C*). In contrast, the effect of pyrophosphate on the affinity for dUMP was negligible suggesting that a single phosphate group is sufficient to induce closure of the enzyme, as would be expected given that dUMP is an inhibitor of the dimeric dUTPases. Inspection of the interactions between the protein and dUpNpp reveals that of the 13 hydrogen bonds between protein and ligand, four are directed toward the α-phosphate group, three toward the β-phosphate, and none toward the γ-phosphate, with the remainder involved in binding to the uracil ring and deoxyribose moieties. Further contribution comes from the active site metals, one of which coordinates to the α-phosphate group, and this region does indeed appear to be very important for substrate binding. It would therefore appear that any compounds that are likely to induce closure and inhibit dimeric dUTPases must bear a suitable negative charge that would enable them to interact efficiently with the phosphate-binding region.

Conclusions—The fact that structures of the dUTPases from trypanosomes are vastly different from the human trimeric enzymes makes them an attractive drug target for the development of new drugs against the diseases caused by these organisms. We have determined structures of the enzyme from *L. major* in complex with substrate analogues (dUpNpp and dUpNp), the product dUMP, and a substrate fragment (dU). The resulting information reveals a very tight ligand-binding pocket in this family of dUTPases with little room for modifications of the uracil and ribose rings without perturbation of binding features. The structures in complex with dUMP and dU revealed the presence of sulfate ions in the active site. In the dU complex, a sulfate was observed binding in a position between that taken up by the α- and β-phosphates of the larger substrate analogues, and, in line with this observation, binding data showed that affinity for dU was dependent on PP_i. Taken together, the structural and biophysical evidence indicates that the presence of a single phosphate or similarly charged group is important to induce closure and formation of a high affinity conformation of the enzyme. Work is ongoing to try and develop new inhibitors of these enzymes that exploit these observations and are amenable to use as anti-trypanosomals.

Acknowledgments—We thank Dr. Andrew Leech for assistance with the tryptophan fluorescence quenching data analysis. We acknowledge the Diamond Light Source (beamline IO4) and the European Synchrotron Radiation Facility (beamlines ID29, ID14.2, and BM14) for provision of x-ray data collection facilities. We thank Johan Turkenburg and Sam Hart for assistance with data collection.

REFERENCES

1. Desjeux, P. (1996) *Clin. Dermatol.* **14,** 417–423
2. Shlomai, J., and Kornberg, A. (1978) *J. Biol. Chem.* **253,** 3305–3312
3. Pearl, L. H., and Savva, R. (1996) *Nat. Struct. Biol.* **3,** 485–487
4. el-Hajj, H. H., Zhang, H., and Weiss, B. (1988) *J. Bacteriol.* **170,** 1069–1075
5. Gadsden, M. H., McIntosh, E. M., Game, J. C., Wilson, P. J., and Haynes, R. H. (1993) *EMBO J.* **12,** 4425–4431
6. Hidalgo-Zarco, F., and González-Pazanowska, D. (2001) *Curr. Protein Pept. Sci.* **2,** 389–397
7. Castillo-Acosta, V. M., Estévez, A. M., Vidal, A. E., Ruiz-Perez, L. M., and González-Pacanowska, D. (2008) *Int. J. Biochem. Cell Biol.* **40,** 2901–2913
8. Persson, R., Cedergren-Zeppezauer, E. S., and Wilson, K. S. (2001) *Curr. Protein Pept. Sci.* **2,** 287–300
9. Barabás, O., Pongrácz, V., Kovári, J., Wilmanns, M., and Vértessy, B. G. (2004) *J. Biol. Chem.* **279,** 42907–42915
10. Dauter, Z., Persson, R., Rosengren, A. M., Nyman, P. O., Wilson, K. S., and Cedergren-Zeppezauer, E. S. (1999) *J. Mol. Biol.* **285,** 655–673
11. Kovári, J., Barabás, O., Takács, E., Békési, A., Dubrovay, Z., Pongrácz, V., Zagyva, I., Imre, T., Szabó, P., and Vértessy, B. G. (2004) *J. Biol. Chem.* **279,** 17932–17944
12. Mustafi, D., Bekesi, A., Vertessy, B. G., and Makinen, M. W. (2003) *Proc. Natl. Acad. Sci. U.S.A.* **100,** 5670–5675
13. McGeoch, D. J. (1990) *Nucleic Acids Res.* **18,** 4105–4110
14. Galperin, M. Y., Moroz, O. V., Wilson, K. S., and Murzin, A. G. (2006) *Mol. Microbiol.* **59,** 5–19
15. Hidalgo-Zarco, F., Camacho, A. G., Bernier-Villamor, V., Nord, J., Ruiz-Pérez, L. M., and González-Pacanowska, D. (2001) *Protein Sci.* **10,** 1426–1433
16. Larsson, G., Nyman, P. O., and Kvassman, J. O. (1996) *J. Biol. Chem.* **271,** 24010–24016
17. Camacho, A., Hidalgo-Zarco, F., Bernier-Villamor, V., Ruiz-Pérez, L. M., and González-Pacanowska, D. (2000) *Biochem. J.* **346,** 163–168
18. Harkiolaki, M., Dodson, E. J., Bernier-Villamor, V., Turkenburg, J. P., González-Pacanowska, D., and Wilson, K. S. (2004) *Structure* **12,** 41–53
19. Moroz, O. V., Harkiolaki, M., Galperin, M. Y., Vagin, A. A., González-Pacanowska, D., and Wilson, K. S. (2004) *J. Mol. Biol.* **342,** 1583–1597
20. Beese, L. S., and Steitz, T. A. (1991) *EMBO J.* **10,** 25–33
21. Steitz, T. A. (1993) *Curr. Opin. Struct. Biol.* **3,** 31–38
22. Fogg, M. J., and Wilkinson, A. J. (2008) *Biochem. Soc Trans.* **36,** 771–775
23. Vagin, A., and Teplyakov, A. (1997) *J. Appl. Crystallogr.* **30,** 1022–1025
24. Murshudov, G. N., Vagin, A. A., and Dodson, E. J. (1997) *Acta Crystallogr. D Biol. Crystallogr.* **53,** 240–255
25. Lamzin, V. S., and Wilson, K. S. (1993) *Acta Crystallogr. D Biol. Crystallogr.* **49,** 129–147
26. Emsley, P., and Cowtan, K. (2004) *Acta Crystallogr D Biol. Crystallogr.* **60,** 2126–2132
27. Leslie, A. G. (1999) *Acta Crystallogr D Biol. Crystallogr.* **55,** 1696–1702
28. CCP4 (1994) *Acta Crystallogr. D* **50,** 760–763
29. Painter, J., and Merritt, E. A. (2006) *Acta Crystallogr. D Biol. Crystallogr.* **62,** 439–450
30. Davis, I. W., Leaver-Fay, A., Chen, V. B., Block, J. N., Kapral, G. J., Wang, X., Murray, L. W., Arendall, W. B., 3rd, Snoeyink, J., Richardson, J. S., and Richardson, D. C. (2007) *Nucleic Acids Res.* **35,** W375–383
31. Otwinowski, Z., and Minor, W. (1997) *Methods Enzymol.* **276,** 307–326

32. Ortiz-Salmerón, E., Yassin, Z., Clemente-Jimenez, M. J., Las Heras-Vazquez, F. J., Rodriguez-Vico, F., Barón, C., and García-Fuentes, L. (2001) *Eur. J. Biochem.* **268,** 4307–4314
33. Harding, M. M. (2001) *Acta Crystallogr. D Biol. Crystallogr.* **57,** 401–411
34. Téllez-Sanz, R., Yassin, Z., Bernier-Villamor, V., Ortiz-Salmerón, E., Musso-Buendia, J. A., Barón, C., Ruíz-Pérez, L. M., González-Pacanowska, D., and García-Fuentes, L. (2007) *Biochimie* **89,** 972–980
35. Potterton, L., McNicholas, S., Krissinel, E., Gruber, J., Cowtan, K., Emsley, P., Murshudov, G. N., Cohen, S., Perrakis, A., and Noble, M. (2004) *Acta Crystallogr. D Biol. Crystallogr.* **60,** 2288–2294
36. Bond, C. S., and Schüttelkopf, A. W. (2009) *Acta Crystallogr. D Biol. Crystallogr.* **65,** 510–512

The Crystal Structure of the *Leishmania major* Deoxyuridine Triphosphate Nucleotidohydrolase in Complex with Nucleotide Analogues, dUMP, and Deoxyuridine

Glyn R. Hemsworth, Olga V. Moroz, Mark J. Fogg, Benjamin Scott, Cristina Bosch-Navarrete, Dolores González-Pacanowska and Keith S. Wilson

J. Biol. Chem. 2011, 286:16470-16481.
doi: 10.1074/jbc.M111.224873 originally published online March 15, 2011
